Fourier analysis for hydrostatic pressure sensing in a polarization-maintaining photonic crystal fiber

Paul Childs,[1,2,*] Allan C. L. Wong,[3] H. Y. Fu,[4] Yanbiao Liao,[1] Hwayaw Tam,[4] Chao Lu,[3] and P. K. A. Wai[3]

[1]Department of Electronic Engineering, Tsinghua University, Beijing, China 100084

[2]Currently with the Institute of Electronic Structure and Laser, Foundation for Research and Technology—Hellas, P.O. Box 1527, Heraklion, 711-10 Crete, Greece

[3]Department of Electronic and Information Engineering, Hong Kong Polytechnic University, Kowloon, Hong Kong SAR, China

[4]Department of Electrical Engineering, Hong Kong Polytechnic University, Kowloon, Hong Kong, China

*Corresponding author: pchilds@physics.org

Received 15 October 2010; revised 8 November 2010; accepted 8 November 2010; posted 8 November 2010 (Doc. ID 136670); published 14 December 2010

.We measured the hydrostatic pressure dependence of the birefringence and birefringent dispersion of a Sagnac interferometric sensor incorporating a length of highly birefringent photonic crystal fiber using Fourier analysis. Sensitivity of both the phase and chirp spectra to hydrostatic pressure is demonstrated. Using this analysis, phase-based measurements showed a good linearity with an effective sensitivity of 9.45 nm/MPa and an accuracy of ±7.8 kPa using wavelength-encoded data and an effective sensitivity of −55.7 cm^{-1}/MPa and an accuracy of ±4.4 kPa using wavenumber-encoded data. Chirp-based measurements, though nonlinear in response, showed an improvement in accuracy at certain pressure ranges with an accuracy of ±5.5 kPa for the full range of measured pressures using wavelength-encoded data and dropping to within ±2.5 kPa in the range of 0.17 to 0.4 MPa using wavenumber-encoded data. Improvements of the accuracy demonstrated the usefulness of implementing chirp-based analysis for sensing purposes.

OCIS codes: 060.2370, 060.5295, 070.4340, 120.5475.

1. Introduction

Photonic crystal fibers (PCFs) [1,2] are a particular kind of optical waveguide that confine light with a microstructured lattice that either acts as an effective medium, offering a lower refractive index cladding (like conventional fiber), or provides an optical stop band, that spatially restricts the guided mode from entering it and leaking out. Despite their drawbacks compared to conventional optical fiber, such as having a high insertion loss and cost as well as the difficulty of coupling and fabricating fiber components, there are many available advantages, such as being single mode over the entire transparency range of silica [3], enabling evanescent interaction in the hole structure [4], having low bending loss and the capability for high birefringence and optical nonlinearities. For certain sensing applications, these advantages make them the much more desirable choice.

Hydrostatic pressure (i.e., pressure that acts uniformly with respect to the azimuthal direction) acting on a length of PCF will deform the positioning and eccentricity of the hole structure, changing the birefringence [5]. Using birefringent PCF, where there is an asymmetry in the hole structure of the photonic crystal [6], gives an offset to this birefringence and improves the sensitivity. Birefringent PCF is generally made entirely from pure silica, and it

0003-6935/10/366861-07$15.00/0

offers the ability to perform temperature-insensitive measurements [7] unlike PANDA and bow tie designs where the thermal properties of the different component materials vary. In addition, the birefringence of highly birefringent PCF is typically 1 order of magnitude larger than that of conventional high-birefringent fiber [6]—permitting both greater pressure sensitivity and reduced temperature cross sensitivity.

The birefringent properties of a fiber would normally be measured using polarimetric detection. Polarimetric detection, however, is generally undesirable as it requires components for polarization control that add to the system complexity and cost. An alternate method is found in using a Sagnac loop, where the polarization states are different for the two propagation paths [8], and so the birefringence creates an optical phase difference that can be measured from the wavelength-encoded interference spectrum. As birefringent PCF offers reduced bend-induced coupling between the polarization states, small compact Sagnac loops are possible.

Fourier analysis is widely used for digital postprocessing, e.g., in such applications as image processing, acoustics, and oceanography. The discrete Fourier transform takes a sampled spectrum and converts it into a dual domain where the individual frequency components can be directly analyzed. In the field of optical fiber sensing, it is used to analyze the spectra of interferometric sensors to determine properties such as the gap length of Fabry–Perot sensors [9], as well as providing an additional domain over which to perform multiplexing [10,11].

In this paper, Fourier analysis is used to experimentally examine the response of the phase shift and chirp in the interference of a Sagnac interferometer comprised of highly birefringent PCF to an applied hydrostatic pressure. The accuracy of the two methods for determining pressure is compared as is the use of interpolation to perform Fourier analysis on the wavenumber domain data.

2. Theory

We start by modeling the interference spectrum of any interferometer as a Taylor expansion over the measured domain variable D (wavelength λ or wavenumber β) as having a phase difference:

$$\psi_D = \phi_{0,D} + \sum_{j=1}^{\infty} k_{j,D}(D - D_0)^j. \tag{1}$$

For the case of a Sagnac interferometer, the optical phase difference is given by [8]

$$\psi = \frac{2\pi}{\lambda} BL, \tag{2}$$

where L is the length of the birefringent fiber in the interferometer and the birefringence, B, is defined as the difference between the effective refractive indices of the respective slow and fast orthogonal polarization states as $B = n_s - n_f$.

The higher order $k_{j,D}$ terms can thus be seen to be incrementally related to the higher order differentials of the birefringence. Working in the wavenumber domain, this relation is one of proportionality, and

$$k_{j+1,\beta} = \frac{L}{j!}\frac{d^j}{d\beta^j} B(\beta)\bigg|_{\beta=\beta_0}, \tag{3}$$

where the single bar and subscripted expression $\beta = \beta_0$ imply a substitution of β_0 for β in the expression to the left of the bar. In order to apply Fourier analysis for this domain; however, sampling either needs to be linear in the wavenumber domain or interpolated onto a linearly sampled set.

Working in the wavelength domain, it is the more complex series of differentials:

$$k_{j+1,\lambda} = \frac{2\pi L}{j!}\frac{d^j}{d\lambda^j}\frac{B(\beta)}{\lambda}\bigg|_{\lambda=\lambda_0}. \tag{4}$$

Conventionally, changes in the period ($\tau_\beta = 2\pi/BL = 2\pi/k_{1,\beta}$, $\tau_\lambda = \lambda^2/BL = 2\pi\lambda/k_{1,\lambda}$) or the more sensitive phase shift ($\Delta D_0 = \pm(D_0/\tau_D)\Delta\tau_D$) of the measured spectrum are used to determine measurand-induced changes. However, theoretical analysis of the hydrostatic pressure acting on highly birefringent PCF has shown that the group modal birefringence:

$$G = B - \lambda\frac{dB}{d\lambda} = -\lambda^2\frac{k_{2,\lambda}}{2\pi L}, \tag{5}$$

is slightly more sensitive than that of the phase modal birefringence, B [5]. On this basis, it is expected to be useful to investigate the higher order $k_{j,D}; j \geq 2$ terms for their potential to improve the sensitivity over conventional analysis. In order to extract these terms, we make use of Fourier analysis.

The Fourier dual representation of the interference spectrum given by Eq. (1) in the inverse domain, s, is given by

$$\mathcal{F}(\cos\psi_D) = \frac{1}{2}e^{2\pi i D_0 s}\left[e^{i\phi_{0,D}}\delta\left(s - \frac{k_{1,D}}{2\pi}\right) * \sqrt{\frac{\pi}{k_{2,D}}}e^{-i\left(\frac{\pi^2 s^2}{k_{2,D}} - \frac{\pi}{4}\right)} * \frac{2\pi}{\sqrt[3]{3k_{3,D}}}\mathrm{Ai}\left(\frac{-2\pi s}{\sqrt[3]{3k_{3,D}}}\right) * \cdots + \text{h.c.}\right], \tag{6}$$

where $\delta(s)$ is the Dirac delta function, $*$ is the convolution operator, $\mathrm{Ai}(s)$ is the Airy function of the first kind, and h.c. denotes the terms required to maintain Hermitian symmetry (conjugation and reversal in s). This equation is further modified by the inclusion of a DC peak proportional to $\delta(s)$ due to the DC offset of the entire spectrum as well as convolution with the Fourier transform of the envelope function (the envelope function is the function in the wavelength

or wavenumber domain that band limits the interference by modulating it).

It can be seen that the coefficients of the series given in Eq. (1) can be found by isolating the individual terms of Eq. (6). The phase term outside the brackets is the factor most readily used to obtain accurate measurand-induced shifts in the resonant wavelength/wavenumber of an optical sensor spectrum. It can be calculated accordingly as [10]

$$D_0 = -\frac{1}{2\pi}\frac{\overline{d\Phi_D}}{ds}, \tag{7}$$

where Φ_D is the phase spectrum of the Fourier transform of $\cos\psi_D$ and the overbar represents taking a weighted average of the property over the range of the harmonic peak corresponding to the convolved delta function of Eq. (6). For optimal results, the weight is taken as the magnitude spectrum of the peak (either in its initial state to ensure stability or its current state to allow a measure of adaptive processing).

The peak location of the delta function of Eq. (6) can also be used to determine the period of the interference, τ_D, which also experiences measurand-induced changes. Its sensitivity is less than that of the wavelength shift (as $\tau_D/D_0 \ll 1$) and is not of as much value except in its use in determining other terms. As such, for the purpose of determining the measurand, an analysis of $k_{1,D}$ is made obsolete by an analysis of D_0 and will not be performed herein. Nevertheless, a stable method for determining the period of the interference is obtained via the expectation value:

$$k_{1,D} = 2\pi\frac{\sum M_D s}{\sum M_D}, \tag{8}$$

where M_D is the magnitude spectrum and the summation is performed over the harmonic peak.

The higher order terms are generally of limited usefulness and, to the best extent of our knowledge, have not been applied to optical fiber sensing to date. Their effects can readily be seen in that the harmonic peak is wider than the DC peak centered at zero. Whereas the DC peak is broadened by the transform of the envelope alone, the harmonic peak is broadened by the transform of the envelope as well as the higher order terms. For interference fringes without much chirp, there is not much difference between the peaks, but for fringes with a large amount of chirp, such as with cascaded or self-interfering long-period gratings, there is a significant amount of broadening visible in the harmonic peak.

Individually, the higher order terms of Eq. (6) are not band limited. However, due to their rapid oscillatory nature in s, convolution with each other (and the transform of the envelope) effectively band limits each of them to only a few cycles. This allows convergence of the series of terms in Eq. (6), provided there is sufficient convergence of the series in Eq. (1).

The second-order term can be obtained similarly to that of the wavelength shift as

$$k_{2,D} = -2\pi^2\left[\frac{\overline{d^2\Phi_D}}{ds^2}\right]^{-1}. \tag{9}$$

The third-order term is not so simply obtained due to the nature of the Airy function. Its extraction is beyond the scope of this article and, hopefully, will be addressed in future research. A rough qualitative approach would be to measure the degree of odd symmetry about $s = k_{1,D}/2\pi$ in the magnitude spectrum, as the magnitude spectrum of the even order terms and the transform of the envelope are all even symmetric, whereas the Airy function has both even and odd symmetric components that retained their symmetry when convolved with an even symmetric function.

As this third term is asymmetric in s (the Airy function being weighted more heavily on the negative s side), it will introduce a skew in Eq. (8) for determining the value of $k_{1,D}$. This skew will introduce errors in $k_{1,D}$ and will also induce errors in D_0, as the weighted average in Eq. (7) no longer symmetrically cancels out the differential of the $\pi^2 s^2/k_{2,D}$ phase term as well as higher order terms. An expectation of the error induced in D_0 is independent of the weight chosen to evaluate Eq. (7), provided it has even symmetry about the center of the harmonic peak. The upper limit of the error ΔD_0 in this case is given by

$$|\Delta D_0| < \left|\frac{\Delta k_{1,D}}{2k_{2,D}} + O(k_{4,D})\right|, \tag{10}$$

where $\Delta k_{1,D}$ is the skew error in $k_{1,D}$ introduced from the asymmetry of the higher order odd terms of Eq. (6) and the inequality is due to the aforementioned damping out of the rapidly oscillating higher order terms in s by convolution with the transform of the envelope—reducing its influence in the differential in Eq. (7). A solution to reduce this error would be to use an asymmetrically weighted average based on the asymmetry in the magnitude spectrum. Further research will attempt to address this.

Changes to the birefringence, and its differentials, can be readily measured using Eqs. (7)–(9), (3), and (4) above. The following experimental investigation is made to compare the appropriateness of using the higher order terms $k_{2,D}$ to that of the conventional analysis of D_0.

3. Experiment

We spliced 60 cm of polarization-maintaining PCF (PM-1550-01, Blaze Photonics) to two ports on the same side of a 3 dB coupler [12]. A cross section of the fiber is shown in Fig. 1. Birefringence can be seen to be due to having two larger holes on opposite sides of the core. The fiber has a pitch length (hole spacing) of 4.4 and hole diameters of 2.2 μm and 4.5 μm for the

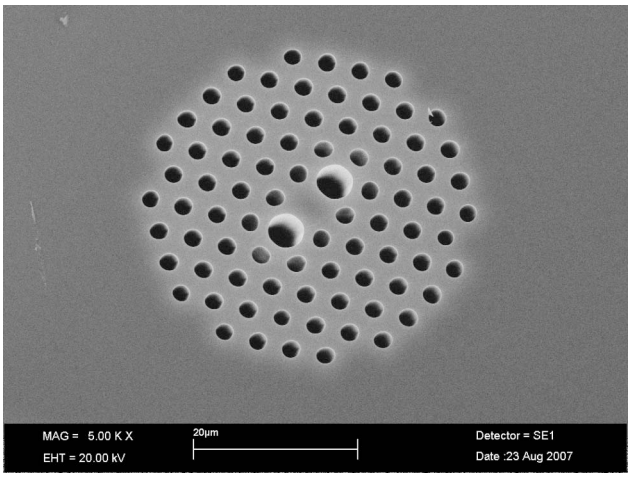

Fig. 1. Cross section of the polarization-maintaining PCF used as a pressure sensor [14].

normal and larger holes, respectively. Light was launched into one of the remaining ports of the coupler using a superluminescent diode (SLD) pair (DenseLight Semiconductors DL-CS48H5A and DL-CS6107A) and the spectrum measured from the other with an optical spectrum analyzer (Agilent 86140B). As the Sagnac loop is polarization independent [13] and good visibility of the interference was seen, no further polarization control was necessary for the experimental setup beyond use of the polarization-maintaining PCF.

The sensor was placed in a sealed chamber and exposed to pressures in the range of 0.1 to 0.4 MPa, which were monitored using a pressure gauge (COMARK C9557). Pressure was applied using an air compressor with an attached regulator. Using the regulator, the pressure level could be accurately controlled and maintained. A reference reading of the spectrum of the SLD pair was taken to give a baseline for transmission measurements.

Two sets of experiments were performed to establish the behavior of the sensor. The first set was performed to establish the response of the sensor; the pressure being varied smoothly; lowering from 0.4 to 0.1 MPa. The second set was performed at a fixed set of pressures so as to better quantify the accuracy limitations of the sensor.

Measurements of the transmission spectra of the Sagnac interferometer at the various pressures were

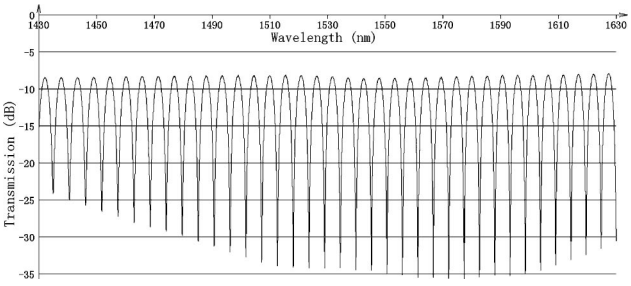

Fig. 2. Transmission spectrum of the polarization-maintaining PCF-based Sagnac interferometer at 0.4 MPa pressure.

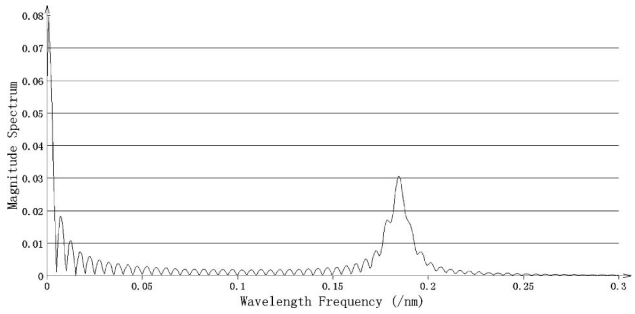

Fig. 3. M_λ, magnitude of the Fourier transform of the sensor spectrum over the wavelength at 0.4 MPa of pressure.

collected for the first set of experiments. Figure 2 shows such a spectrum for the case where the pressure was 0.4 MPa. Fourier transforms of the (wavelength-domain-based) spectra were calculated and can be seen in the overall magnitude spectrum for one measurement presented in Fig. 3 and the phase spectra near $s = k_{1,\lambda}/2\pi$ for the full set of measurements in Fig. 4. Ringing is seen on the magnitude spectrum in Fig. 3 due to zero padding the wavelength domain by a factor of 8 (i.e., 2^{16}–2^{13} points of zero value are added on after the 2^{13} points of the measured spectrum) to give a sufficient number of data points in the Fourier domain for the following analysis [this zero padding corresponds to an interpolation in the Fourier domain giving 8 times the number of points to average over in Eqs. (7)–(9)]. As this ringing effect has a zero phase, it does not disrupt the measurements of D_0 and $k_{2,D}$ in any way.

All the measured spectra were then interpolated to give a linear sampling rate in the wavenumber domain. Fourier transforms were calculated, and the overall magnitude spectrum for one measurement and the phase spectra near $s = k_{1,\beta}/2\pi$ for the full set of measurements are presented in Figs. 5 and 6, respectively.

The terms λ_0 and $k_{2,\lambda}$, for data represented in the wavelength domain, were determined for each measurement using Eqs. (7) and (9). A graph of these two properties with respect to pressure is presented in Figs. 7 and 8, respectively. Similarly, for data represented in the wavenumber domain, the terms β_0 and $k_{2,\beta}$ were determined and are presented in Figs. 9 and 10, respectively.

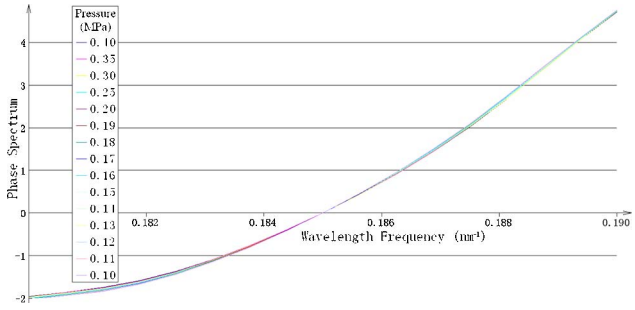

Fig. 4. (Color online) Φ_λ, Phase of the Fourier transform of the sensor spectra over the wavelength (inset, pressure in MPa).

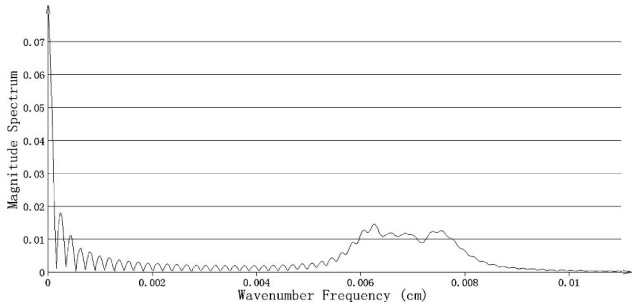

Fig. 5. M_β, magnitude of the Fourier transform of the sensor spectrum over the wavenumber at 0.4 MPa of pressure.

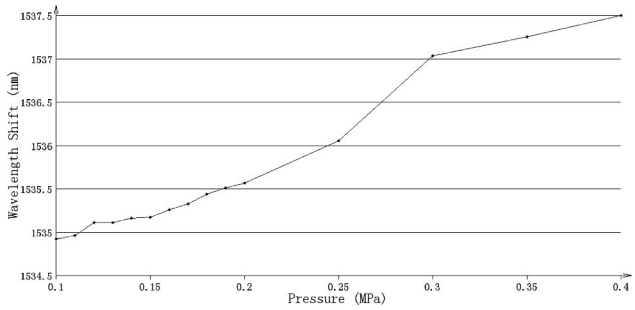

Fig. 7. Variation of the parameter λ_0 with respect to pressure.

For the second set of experiments (that of quantifying the accuracy of measurement), further testing was performed by holding the pressure at 0.11, 0.13, 0.196, 0.308, and 0.4 MPa over a time period of 8 min each and monitoring the stability of the spectrum. Five measurements were taken at each pressure during these time periods. On average, the phase was measured to fluctuate with a standard deviation of $\Delta\lambda_0 = 74$ pm and the chirp, accordingly, as $\Delta k_{2,\lambda} = 8.4 \times 10^{-8}$ nm^{-2}. Variation was seen in the amount of fluctuation at each pressure, suggesting that a large component of the variation was due to the pressure stability of the chamber rather than being intrinsic to the measurement scheme. Nonetheless, it sufficed for comparing the difference between measurement methodologies. On average there was no general trend seen with respect to pressure except for the case of the chirp measurements where greater fluctuation was seen at higher pressures. Similar results for analysis performed in the wavenumber domain gives $\Delta\beta_0 = 0.25$ cm^{-1} and $\Delta k_{2,\beta} = 8.2 \times 10^{-10}$ cm^2, again with greater fluctuation being seen at higher pressures in the chirp measurements.

4. Discussion

There are three readily identifiable causes for chirp in the interference spectrum. The first is due to the measurement being carried out in a domain that naturally gives rise to chirp (e.g., wavelength) due to the interference in it being nonlinearly related to beat length. This can be avoided by transforming to the wavenumber domain where there is a linear relation. The second cause is due to dispersion in the fiber, and it is this cause that is investigated for pressure sensing.

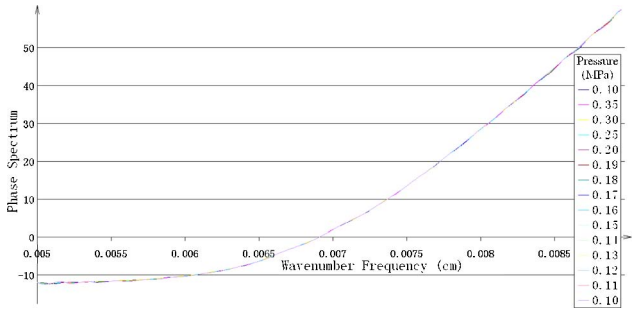

Fig. 6. (Color online) Φ_β, phase of the Fourier transform of the sensor spectra over the wavenumber (the inset is the pressure in MPa).

The final cause is due to any possible changes in the measurand as the spectrum is scanned; the primary cause being air leaking out of the chamber. The rate of leakage is proportional to the pressure differential between the inside and outside of the chamber, ΔP, giving differentials for the pressure: $dP/dt = -\alpha\Delta P$ and $d^2P/dt^2 = \alpha^2\Delta P$. Given a positive sweep rate, $d\lambda/dt = R$, and phase sensitivity, $d\phi/dP = \sigma$, the induced detuning, $d\phi/d\lambda$, and chirp, $d^2\phi/d\lambda^2$, are negatively and positively valued, respectively, causing a decrease in λ_0 (as opposed to what is seen in Fig. 7) and an increase in $k_{2,\lambda}$ with applied pressure. For small leaks ($\alpha\lambda_0 \ll R$), the former effect is greater than the latter, and, as such, the effect on chirp is minimal and cannot account for what is seen in Fig. 8.

The existence of chirp and higher order dispersion in the interference can readily be seen in Fig. 3, where the harmonic peak has been significantly broadened over what is the case for the DC peak. The even order chirp terms can be directly seen in the nonlinearity of the phase spectrum in Figs. 4 and 6.

Although, visually, there is not much change in the phase (or, for that matter, the magnitude) of the Fourier spectra, it can still be seen in Figs. 4 and 6 that the changes to the chirp and higher order factors outweigh the changes to the linear phase slope.

From Eq. (5) and the results of Fig. 8, it can be seen that the group modal birefringence decreases with pressure, in agreement with what has been shown to be the case using finite element modeling for this fiber geometry [5]. Considering that changes to $k_{1,\beta}$

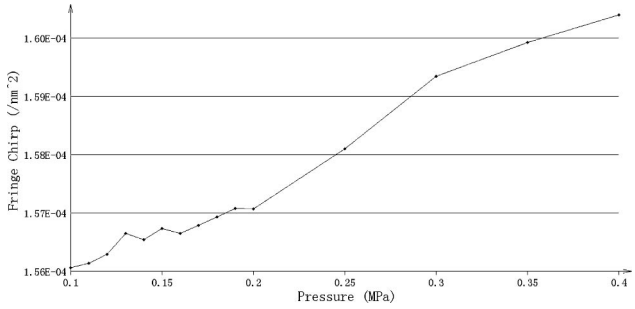

Fig. 8. Variation of the parameter $k_{2,\lambda}$ with respect to pressure.

are inversely proportional to changes in β_0, Eq. (3) and the results of Fig. 9 show that the phase modal birefringence increases with pressure, contrary to what is presented in [5], where dB/dP is claimed to be negative. The positive value found herein was further confirmed by visually identifying the resonances of the spectrum shifting to a lower wavenumber/higher wavelength with an increase in pressure in agreement with previous experimental studies [14,15].

From Fig. 7 we see that the phase-based measurement for λ_0 varies more or less linearly with applied pressure, which has been shown to be the case theoretically and experimentally earlier [13]. No such theoretical relation exists for $k_{2,D}$, and the linearity seen in Fig. 8 will not necessarily be the case for all pressure ranges or fiber types.

Linear fits to the data in Figs. 7–10 give the respective sensitivities of 9.45 nm/MPa, 1.54×10^{-5} nm^{-2}/MPa, -55.7 cm^{-1}/MPa, and 3.22×10^{-7} cm^2/MPa. The Pearson R^2 values, describing how well the linear trends fit, are 0.97, 0.98, 0.98, and 0.94, respectively, showing good linearity for all but $k_{2,\beta}$, the linear chirp based on data expressed in the wavenumber domain. Owing to this nonlinearity, the response is better characterized as having a linear sensitivity of 7.87×10^{-8} cm^2/MPa for pressures below 0.17 MPa and a quadratic dependence on the pressure in megapascal, P, as $(8.17 \times 10^{-7} \cdot P^2 - 6.04 \times 10^{-8} \cdot P)$ cm^2 above it. This latter dependence inverts to give $\Delta P = (-2.26 \times 10^{13} \Delta k_{2,\beta} + 3.46 \times 10^7) \Delta k_{2,\beta}$ MPa.

The calculated sensitivities are much larger than what is observed by making direct observations of the shift of the fringes in the wavelength and wavenumber domains (the dip near 1530 nm varies by only 0.977 nm over the whole 0.3 MPa range). This is due to the asymmetry of the third-order term shifting the measured location of the harmonic peak from the true value of $k_{1,D}/2\pi$, as was discussed in the theory above concerning Eq. (10). From Figs. 4 and 6 it can be seen that the phase slope varies strongly with the frequencies in nanometers^{-1} and centimeters, respectively, and so a small shift in the harmonic peak location will lead to a large change in the phase slope. Any attempt to correct for shifts in the harmonic peak location is not helpful, as the signal-to-noise ratio for measuring the phase is reduced due to a corresponding reduction in the magnitude spectrum

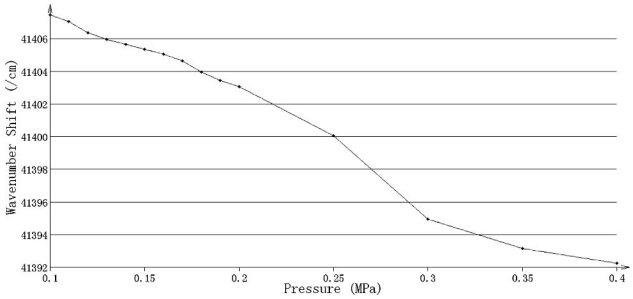

Fig. 9. Variation of the parameter β_0 with respect to pressure.

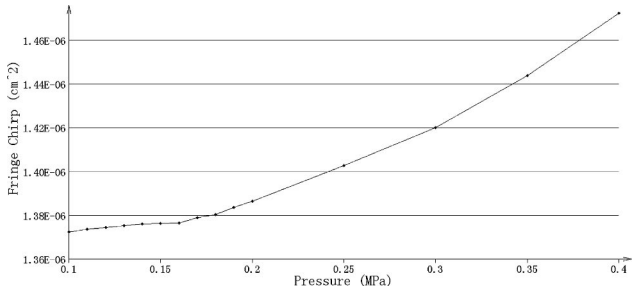

Fig. 10. Variation of the parameter $k_{2,\beta}$ with respect to pressure.

when measuring offset from the center of the harmonic peak. As such, it is best to measure the phase with the harmonic peak as is and calibrate out the difference; keep in mind the obtained shifts are not the true values, but as this is only an intermediate value in determining the pressure and provided that the behavior is repeatable, then it will not be a problem.

Based on the stability measurements performed at the end of the experimental section, the above linear fits would imply accuracies for measuring pressure of ± 7.8 kPa and ± 5.5 kPa for wavelength domain measurements based on linear phase and chirp, respectively, and ± 4.4 kPa and ± 2.5 kPa for wavenumber domain measurements based on linear phase and chirp, respectively. However, owing to the nonlinearity of Fig. 10, this latter value for the accuracy does not adequately quantify it well throughout. In the linear region at low pressures below 0.17 MPa, the accuracy is measured to be ± 7.9 kPa, whereas at pressures above 0.17 MPa the accuracy was within ± 2.5 kPa throughout.

Whereas measurements of the wavelength shift guarantee linearity of response and offer simplicity of analysis, the results show that better accuracy may be obtained by measuring the birefringent dispersion obtained using Fourier analysis from the chirp of the phase spectrum. With proper calibration of the sensor response, the improvement in accuracy obtained definitely makes the increase in complexity worthwhile. Similarly, converting the measured spectrum to a function of the wavenumber introduces the additional complexity of interpolating the dataset; however, the improvement in accuracy clearly makes it also worthwhile.

While performing the analysis, changes in the magnitude spectrum with applied pressure were also noted. Greater variations in the asymmetry about the harmonic peak were seen for the case of performing the analysis in the wavenumber domain. However, a detailed analysis of changes to the higher order terms will require further theoretical work, and it is likely to be of less use, owing to the expected limited accuracy and stability in calculating them compared to the lower order terms.

5. Conclusion

Fourier analysis was used to measure the wavelength shift and chirp of the interference fringes of

a Sagnac interferometer incorporating a polarization-maintaining PCF. A theoretical formulation for determining the wavelength shift and the linear and quadratic wavelength dependence of the phase was developed. Effective sensitivities were measured as 9.45 nm/MPa, $-55.7\ \mathrm{cm}^{-1}$/MPa, and $1.54 \times 10^{-5}\ \mathrm{nm}^{-2}$/MPa for the analysis of wavelength shifts, wavenumber shifts, and chirp in the wavelength spectrum, respectively. Nonlinearity of the response was seen when an analysis of chirp in the wavenumber-domain-based measurements was performed.

This project was supported in part by the National Natural Science Foundation of China (NSFC) under grant 60629401, in part by the Hong Kong Polytechnic University Grants Committee Matching Grant under project J-BB9J, and in part under project G-YX2C.

References

1. P. Russell, "Photonic crystal fibers," Science **299**, 358–362 (2003).
2. J. C. Knight, "Photonic crystal fibres," Nature **424**, 847–851 (2003).
3. T. A. Birks, J. C. Knight, and P. St. J. Russell, "Endlessly single-mode photonic crystal fiber," Opt. Lett. **22**, 961–963 (1997).
4. T. M. Monroe, W. Belardi, K. Furusawa, J. C. Baggett, N. G. R. Broderick, and D. J. Richardson, "Sensing with microstructured optical fibres," Meas. Sci. Technol. **12**, 854–858 (2001).
5. M. Szpulak, T. Martynkien, and W. Urbanczyk, "Effects of hydrostatic pressure on phase and group modal birefringence in microstructured holey fibers," Appl. Opt. **43**, 4739–4744 (2004).
6. A. Ortigosa-Blanch, J. C. Knight, W. J. Wadsworth, J. Arriaga, B. J. Mangan, T. A. Birks, and P. St. J. Russell, "Highly birefringent photonic crystal fibers," Opt. Lett. **25**, 1325–1327 (2000).
7. D. H. Kim and J. U. Kang, "Sagnac loop interferometer based on polarization maintaining photonic crystal fiber with reduced temperature sensitivity," Opt. Express **12**, 4490–4495 (2004).
8. D. B. Mortimore, "Fiber loop reflectors," J. Lightwave Technol. **6**, 1217–1224 (1988).
9. S. M. Musa, "Real-time signal processing and hardware development for a wavelength modulated optical fiber sensor system," Ph.D. dissertation (Virginia Polytechnic Institute and State University, 1997).
10. P. Childs, "An FBG sensing system utilizing both WDM and a novel harmonic division scheme," J. Lightwave Technol. **23**, 348–354 (2005)..
11. P. Childs, "Erratum to 'An FBG sensing system utilizing both WDM and a novel harmonic division scheme'," J. Lightwave Technol. **23**, 931 (2005).
12. M. L. V. Tse, H. Y. Tam, L. B. Fu, B. K. Thomas, L. Dong, C. Lu, and P. K. A. Wai, "Fusion splicing holey fibers and single-mode fibers: a simple method to reduce loss and increase strength," IEEE Photon. Technol. Lett. **21**, 164–167 (2009).
13. X. Fang and R. O. Claus, "Polarization-independent all-fiber wavelength-division multiplexer based on a Sagnac interferometer," Opt. Lett. **20**, 2146–2148 (1995).
14. H. Y. Fu, H. Y. Tam, L. Y. Shao, X. Dong, P. K. A. Wai, C. Lu, and S. K. Khijwania, "Pressure sensor realized with polarization-maintaining photonic crystal fiber-based Sagnac interferometer," Appl. Opt. **47**, 2835–2839 (2008).
15. H. Y. Fu, A. C. L. Wong, P. A. Childs, H. Y. Tam, Y. B. Liao, C. Lu, and P. K. A. Wai, "Multiplexing of polarization-maintaining photonic crystal fiber based Sagnac interferometric sensors," Opt. Express **17**, 18501–18512 (2009).